Advanced hybrid plasmonic nano-emitters using smart photopolymer

Dandan Ge, Safi Jradi, Christophe Couteau, Sylvie Marguet, Renaud Bachelot

Advanced hybrid plasmonic nano-emitters using smart photopolymer

Dandan Ge,[1] Ali Issa,[1] Safi Jradi,[1,*] Christophe Couteau,[1] Sylvie Marguet,[2] Renaud Bachelot[1,*]

[1] *Light, nanomaterials, nanotechnologies (L2n) Laboratory. CNRS ERL7004. Université de Technologie de Troyes, 12 rue Marie Curie, 10004 Troyes Cedex, France*
[2]*Université Paris Saclay, CEA, CNRS, NIMBE, F-91191 Gif sur Yvette, France*
[3]*safi.jradi@utt.fr,*
[4]*renaud.bachelot@utt.fr*

Abstract: The integration of nano-emitters into plasmonic devices with spatial control and nanometer precision has become a great challenge. In this paper, we report on the use of a smart polymer for selectively immobilizing nano-emitters on specific preselected sites of gold nanocubes (GNC). The cunning use of the polymer is twofold. First, it records both the selected site and the future emitters-GNC distance through plasmon-assisted photopolymerization. Second, because the polymer is chemically functionalized, it makes it possible to attach the nano-emitters right at the preselected polymerized sites which subsequently "recognize" the nano-emitters to get attached. Since the resulting active medium is a spatial memory of specific plasmonic modes, it is anisotropic, making the hybrid nanosources sensitive to light polarization. The ability to adjust their statistical average lifetime by controlling the thickness of the nanopolymer is demonstrated on two kinds of nano-emitters coupled to GNC: doped polystyrene nanospheres and semiconductor colloidal quantum dots.

1. INTRODUCTION

Organic and inorganic nano-emitters are used for many topical applications ranging from nano-optics and nano-photonics to biomedicine and cell biology. [1–3] When weakly or strongly coupled to metal nanoparticles, their key properties can be controlled: (e. g.) lifetime, [4,5] quantum yield, [6] fluorescence directivity, [7] emission intensity, [8] and spectral properties [9]. The integration of these hybrid nano-emitters as optical nanosources into photonic nanodevices is of interest for research and technological innovation due to their miniaturization and multi-applications.

However, the integration of the emitters near metallic nanostructures with spatial control and nanometer precision in the three space dimensions remains a challenge. In the simplest way, the emitters are dispersed randomly on the plasmonic structures, without any position control. [10,11] By adding a spacer layer, the separation distance between the emitters and metallic structures can be controlled along one direction. [12–14] To achieve 3D spatial control of emitters relative to metallic nanostructures, a method based on trapping emitters in an isotropic silica shell covering the entire metallic nanoparticles has been reported. [15,16] Scanning-based methods have been reported to study in a controlled way the coupling between emitters and metallic nanostructures. [17,18] The DNA origami-assisted method, as a powerful approach, has been used for building special plasmonic nanoantennas and linking together plasmonic nanostructures and nano-emitters. [19–22] For the structures presenting a gap, including dimers and particles-film structures, DNA origami has proved to be able to place emitters, even a single one, within the gap. [23–27]. In other words, DNA is generally used for both bridging particles together and attaching nano-emitters. In the case of single metal

nanoparticles, the whole surface of particles is functionalized. With this approach, it is thus difficult to control the anisotropy of the emitters distribution around single plasmonic nanostructures. With the use of a DNA clamp, gold nanoparticles have been placed at three special positions around a single nanorod, but the DNA clamp and special capture strands on the clamp limit the shapes and size of the host nanostructures and it is hard to change capture positions for a defined clamp [28]. Besides, DNA-based hybrid nanosystem are pretty fragile in the sense that, for the survival of DNA origami, one needs to be in a salty liquid environment, which limits the types of available metallic nanoparticles, and requires complicated steps. This environment requirement limits the use of this approach for direct integration into nanophotonic circuits. Although site-selective coating based on anisotropic chemical growth on metal nanostructures was reported, [29–32] there are still challenges in achieving anisotropic distribution of the emitters themselves near metal nanoparticles. As a matter of fact, controlling in the three space dimensions, the anisotropic spatial distribution of emitters in the vicinity of single metal nanostructures still constitutes a challenge.

Near-field plasmonic photopolymerization has proven to be an effective technique to trap light-emitting quantum dots and molecules inside polymer volumes that are integrated at electromagnetic 'hot-spots' [33,34]. The anisotropic distribution of emitters can be controlled by choosing the plasmonic mode used for nanophotopolymerization. However, since the emitters are initially randomly distributed inside the photopolymerizable formulation, the spatial distribution of the emitters is still not precise enough. In particular, the distance between the nano-emitters and the metal nanoparticle in the structures of Ref. 33 is not controlled. In addition, because the emitter is pre-dispersed within the formulation, it is difficult to consider the influence of the curing laser on the emitter during the photopolymerization process, such as the two-photon absorption by the emitters, and the possible light force that may squeeze the emitters outward.

In this letter, we report on the use of a smart nano-polymer that allows us to address the above issues. The smart nature of the polymer is twofold. First, it is a photopolymer that reticulates at the plasmonic hot spot of the metal nanoparticle, allowing one to keep the memory of the selected electromagnetic sites. This "memory" is spatially anisotropic and also decides the distance between the plasmonic nanostructure and the future nano-emitter to be attached. Secondly, it is chemically pre-functionalized to electrostatically "recognize" the nano-emitter that can get selectively attached to the pre-designed sites.

Our approach is actually based on the association of three controlled elements: plasmonic nanostructures, smart photopolymer and nano-emitters.

2. EXPERIMENTAL SECTION

A. Plasmonic nanostructures

The plasmonic nanocavities used are 125-nm gold nanocubes (GNC, Fig. 1(a)) made by chemical synthesis using the method already described in detail in Ref.35. These cubes, deposited on an ITO-coated glass substrate, present a dipolar plasmon resonance at 670 nm in air, see blue curve in Fig. 1(b), suitable for resonant near-field two-photon polymerization. [33]

B. Smart photopolymer

The photopolymer has been designed for plasmon-induced two-photon nanoscale polymerization [33, 34] but has been modified: it is also a functionalized polymer that grabs the emitters to its surface by electrostatic interaction. In that way, we can control both the number of emitters attached to the polymer surface and the average emitter-metal surface distance by adjusting the thickness of the polymer on the plasmonic structure. The

photosensitive formulation consists of 4.99 mmol of Pentaerythritol triacrylate (PETA) monomer functionalized by 2.51 mmol of methyldiethanol amine (MDEA). 0.039 mmol of 2-Isopropylthioxanthone (ITX) was added to absorb light and make interaction with MDEA to initiate the two-photon polymerization reaction and 1.13 mmol of monomethyl ether of hydroquinone (MEHQ) inhibitor was added to control the spatial confinement of the polymerization process. After photo reticulation and development, the polymer surface presents a high density of amino groups 10^8 molecules per μm^2 determined by the orange 2 test.

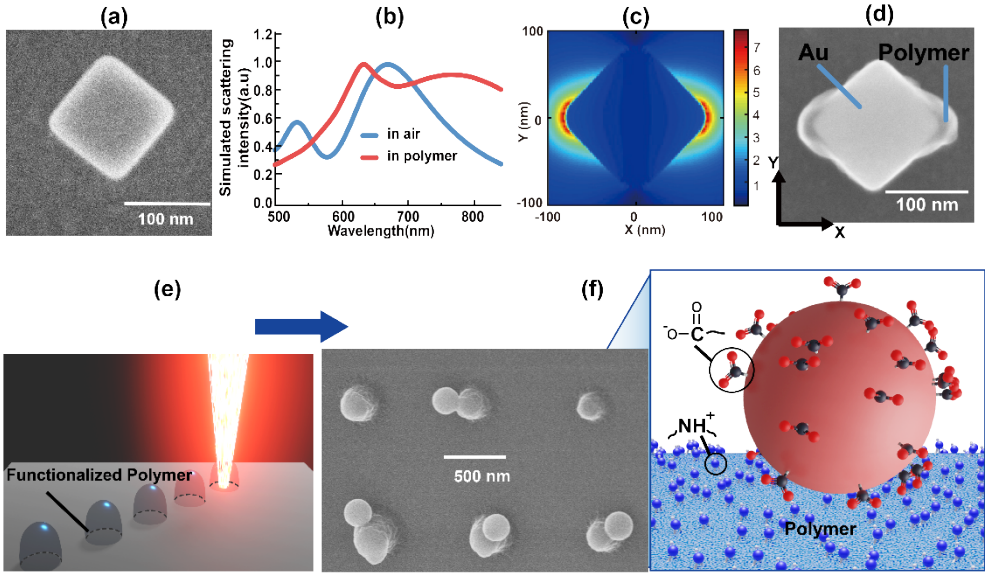

Fig. 1 Gold nanocubes, nanoscale photopolymerization and surface functionalization. (a) SEM image of a representative single gold nanocube. (a) Calculated scattering spectrum of a single gold nanocube of 125-nm, in air or photopolymer medium (refractive index=1.48), on ITO-coated glass substrate (40 nm thickness of ITO layer with refractive index of 2). (b) FDTD map (at the middle sectional plane of the cube, λ=780 nm) of the field modulus in the vicinity of the gold nanocube illuminated with a X-polarized plane wave. (d) SEM image of the hybrid nanostructure resulting from 2-photon polymerization (TPP) triggered by the field shown in (c). (e) Illustration of the photopolymerization of mixture of PETA monomer functionalized by amine. (f). Left: SEM image of polymerized dots whose surface contains amine group. After immersion in a solution of negatively charged functionalized fluorescent doped polystyrene spheres (200-nm diameter), the fluorescent spheres attached on four of the six polymer dots by electrostatic interaction. Right: schematic representation of the electrostatic interaction.

More information about the smart photopolymer can be found in Ref. 36. The obtained polymer nanotemplates are intended to be immersed in acidic medium solution of negatively charged nano-emitters, resulting in the specific attachment of these nano-emitters on the polymer surface. In other words, during immersion, the negatively charged nano-emitters selectively assemble, by electrostatic interaction, on the positively charged functionalized polymer surface due to the presence of protonated amine groups [Fig. 1(f)].

C. Nano-emitters

The first considered nano-emitters are fluorescent polystyrene spheres (FPS, from Thermo Fisher) doped with light-emitting molecules. They are similar to those introduced in Fig. 1 but they are significantly smaller: their average size is 45 nm (see Appendix B). The absorption spectrum presents a peak at 580 nm whereas the emission peak is at 620 nm (see Appendix B). Such FPSs were used by J. de Torres et al. to demonstrate plasmons-mediated fluorescence energy transfer on silver nanowires. [37] The authors deposited the FPSs by spin-coating and their spatial distribution was not controlled. The carboxylate-modified FPSs (FluoSpheres,

model F8793) used in this letter, are negatively charged and thus able to get selectively positioned to the functionalized polymer surface by electrostatic force.

Based on the three above-described elements, advanced hybrid plasmonic nano-emitters can be made.

D. Protocol for fabricating the hybrid plasmonic nano-emitters

The protocol for fabricating the hybrid plasmonic nano-emitter consists of two main steps (Fig. 6).

Step 1. This step consists of the fabrication of the functionalized nanopolymer on the GNC surface by plasmon-triggered polymerization at 780 nm. [33,34,38] This wavelength efficiently excites the GNC plasmon when this later is surrounded by the liquid photopolymer [see red curve in Fig. 1(b)] and is efficiently absorbed by ITX that is used as a 2-photon absorber. [39] The photopolymerization occurs specifically at the electromagnetic hot spots, when the near-field intensity exceeds a certain intensity threshold. During this step, the selected nanoscale sites are thus recorded by the polymer. After exposure, the deposited polymer volume is revealed through rinsing with acetone and isopropanol for 10 mins separately. Fig. 1(d) illustrates a typical hybrid nanocube, revealed after rinsing, that results from nano-polymerization triggered by the plasmonic dipolar eigenmode excited with a X polarization parallel to the diagonal of the cube [Fig. 1(c)]. The process relies on the control of the incident intensity relative to the threshold dose (D_{th}) of 2-photon polymerization. For getting the result shown in Fig. 1(d), the incident laser dose was 40% of the threshold dose, so that no polymerization occurs, except in the near-field of the GNC [illustrated in Fig. 1(c)] where the local dose gets higher than D_{th} through plasmon enhancement.

The used experimental configuration for this step is shown in Appendix A, Fig. 7.

Step2. Following step 1, the sample is immersed into the FPS solution for 40 min. The FPSs were stabilized by carboxylic acid and have negative charges on their surface. During immersion and due to the presence of amine groups on the polymer (positive charges) FPSs get attracted by the polymer, leading to the selective attachment of FPSs on its surface by electrostatic interaction. During this step, the pre-recorded smart polymer gets revealed by selectively attaching nano-emitters.

E. Selective attachment of fluorescent spheres at the nanocube corners

By adjusting the dose used for step 1, we were able to control the nanopolymer's thickness and thus the average distance between the GNC surface and the nano-emitters to be attached. At the same time, increased thickness of polymer leads to the increased number of grafted emitters. Fig. 2 illustrates this point: two different volumes of the polymer lead to a large change in the number of attached FPSs. The effect of the dose on the volume of polymer is clearly shown in Appendix C, Fig. 10. The selective immobilization of FPSs at the two corners of GNC is here successfully demonstrated. The excitation laser used for 2-photon polymerization was X-polarized, resulting in two lobes of smart polymer that took the shape of the local plasmonic field [Fig. 1(c) and 1(d)]. In Fig. 2(a) and 2(b), two identical GNC have been polymerized with two incident doses at 780 nm: 40% and 10% of D_{th}, respectively (step 1). Step 2 results in hybrid FPS/GNC with a number of FPS at each cube corner which is strongly dependent on the dose initially used for step 1: from a tenth of FPSs [Fig. 2(a)] to a few FPSs [Fig. 2(b)]. More examples can be found in Appendix C, Fig. 9. The Appendix H deals with the control of the number of emitters that can attach to the polymer lobes. This number depends on the concentration of emitters in the solution, the size of the emitter, the size of the integrated polymer area and the immersion time. In particular, Fig. 2, Fig. 9 and Fig. 16 illustrate the importance of the latter two.

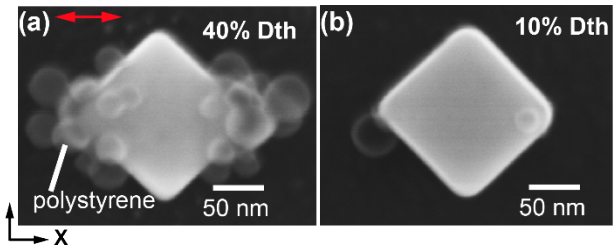

Fig. 2 SEM images of the hybrid FPSs-attached nanostructures fabricated using energy dose of (a) 40% and (b) 10% of threshold during step 1. The red arrow in (a) indicates the polarization direction of the excitation laser used for polymerization during step 1.

3. RESULTS AND DISCUSSION

A. Photoluminescence properties of the resulting hybrid nano-emitters

Under 532 nm excitation, the fluorescent signal was collected through a 650/150 nm band-pass filter (Semrock FF01-650/150-25). The fluorescence spectrum from the hybrid FPS-GNC nano-emitter is shown in Fig. 3(a). In Fig. 3(b), the time trace of fluorescence intensity obtained during 50 s shows no blinking and a pretty good stability of the fluorescence intensity. This is due to the large number of dyes inside each FPS giving out an ensemble signal and the protective environment inside the polystyrene bead isolating the system from the instable effects from the external environment.

These hybrid nanostructures have an anisotropic nanoscale spatial distribution of FPSs that contributes to the polarization sensitivity of their fluorescence intensity. This feature is illustrated in Fig. 3(d). The 532-nm excitation light was linearly polarized with a polarization angle shown in Fig. 3(c). The considered single hybrid nano-emitter has been fabricated during step 1 using 40% of Dth. In Fig. 3(d), the fluorescence intensity decreases when the polarization angle of the excitation laser varies from 0° to 90° and increases when the polarization changes from 90° to 180°. The fluorescence intensity finally goes back to the same intensity level as the intensity of 0°. The switch from high emission signal to weak emission signal is realized by rotating the polarization direction, and a signal contrast δ of about 0.5 is obtained. In Fig. 3(b), the cosine like function, reminding us of the Malus law, is not due to the polarization sensitivity of the GNC. Rather, it is due to anisotropic spatial distribution of the active medium permitted by the smart polymer. More data on the polarization sensitivity can be found in Appendix D.

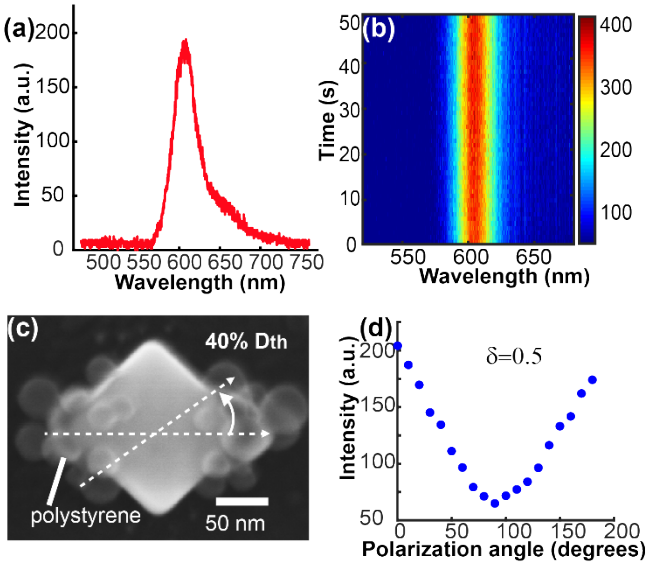

Fig. 3 (a) Fluorescence spectrum measured from the hybrid FPSs-GNC shown in Fig. 2(a) using polarized green laser of 532 nm wavelength for excitation. A 650/150 nm band-pass filter is used to separate the fluorescent signal from the incident excitation (b) Spectrum time trace, collected for 50s. (c) Definition of the polarization angle for excitation. (d) Fluorescence intensity as a function of the angle of incident polarization defined in (c).

B. Control of the average gap between GNC and nano-emitters and resulting Purcell factor

The spatial elongation of the nanopolymer during step 1 can be controlled through incident energy dose. [31, 32] Energy doses ranging from 5% to 70% of D_{th} were used for fabricating hybrid FPSs-attached hybrid plasmonic nanostructures (step 1). The fluorescence lifetime of the FPSs on the hybrid nanostructures, resulting from step 2, was measured to study the influence of the polymer thickness and thus the mean value of the FPS-GNC distance. Fig. 4(a) shows typical lifetime measurements. When the FPSs are directly attached to pure polymer dots without GNC (red curve), the lifetime is longer than it is when the FPSs are attached on the polymer lobes on GNC, which is in agreement with what is expected, i.e., an increase of the radiative and non-radiative deactivation rates in the presence of the metal nanostructure. The lifetime turns out to decrease as the energy dose used for fabrication decreases: green curve (5% D_{th}) demonstrates a much shorter lifetime decay than orange curve (40% D_{th}).

There are hundreds of molecules in each FPS ($3.5x10^2$ fluorescein equivalents per polystyrene sphere). In general, the overall decay of all the molecules can be fitted by a sum of exponential functions [42], *i.e.*,

$$I_{\text{total}}(t) = \sum_{i=1}^{N} A_i \exp(-t/\tau_i), \tag{1}$$

Where N is the number of dyes, $I_{total}(t)$ is the normalized fluorescence intensity at time t from all the FPSs, A_i is the probability density function, and $\sum_i^N A_i = 1$. Parameter i can be viewed as a specific family of molecules that is characterized by lifetime τ_i. The fluorescence lifetime of the FPSs without GNC can be very well fitted using single-exponential function (see Fig.14(a) in Appendix G), suggesting a single family of molecules, with a lifetime in the 6-7 ns range. With the presence of the GNC, the experimental data were fitted by one-exponential, double-exponential and triple-exponential functions. An accurate fit was achieved with double-exponential function, while the third exponential component has near zero probability density (Fig. 14(b)(c), in Appendix G). Hence the whole decay can be expressed as

$$I(t) = a_1 \exp(-\frac{t}{\tau_1}) + (1-a_1)\exp(-\frac{t}{\tau_2}) \tag{2}$$

The double-exponential fitting results with different polymer thicknesses are shown in Fig. 4(b). Clearly, we observe a fast decay τ_1 that is contained in the 1-2 ns range and a slow decay τ_2 which is roughly stable within the 6-7 ns range. Considering the size of the FPS and keeping in mind that several FPSs are attached, we assign the fast decay τ_1 to the contribution of the Purcell effect undergone by the dye molecules, while the slow decay τ_2 is assigned to the emission of unaffected/less affected dye molecules (similar treatment as Ref 43). τ_1 can be seen as the mean value of the fluorescence lifetimes (Eq. 1) of the molecules that are sensitive to the GNC. Coefficient a_1 stands for the weight of this fast decay component. It is associated with the proportion of molecules which undergo the Purcell effect. As shown in Fig. 4(b), a_1 increases when the average polymer thickness decreases. This indicates an increase of the proportion of the dye molecules which are affected by the presence of the GNC, in terms of the Purcell effect.

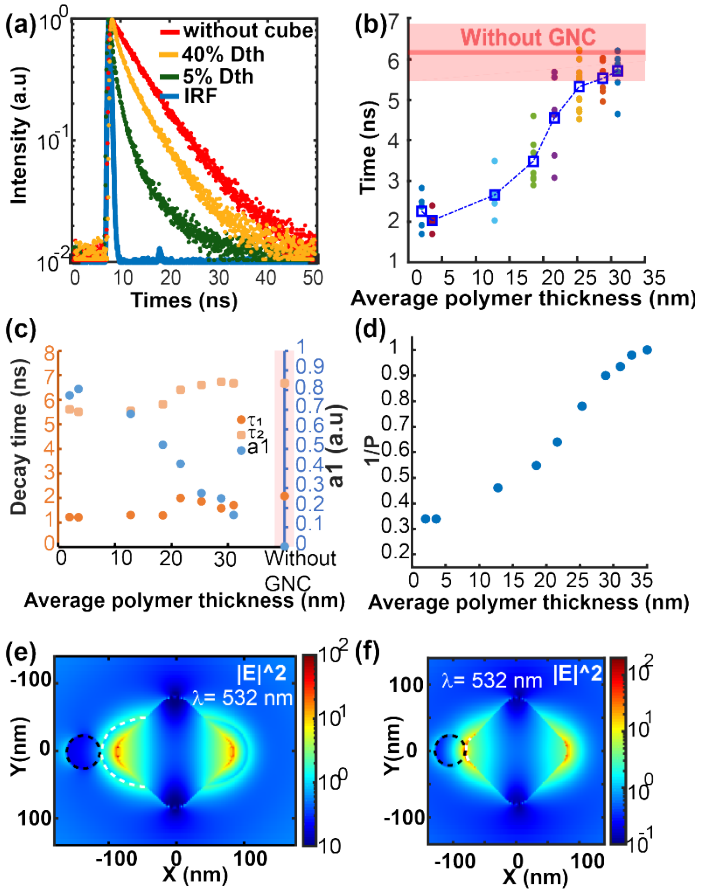

Fig 4 (a) Lifetime measurement of FPSs attached on hybrid polymer-cube fabricated by a dose of 40% D_{th} (orange) and 5% D_{th} (green). (b) Double-exponential fitting results of the lifetime of FPSs: fast decay component τ_1, slow decay component τ_2 and the coefficient a_1 of fast decay component changes as the average polymer thickness varies. (c) Weighted average lifetime of FPSs change along the average distance between the metal surface and FPSs increased by decreasing the incident dose used for fabricating the hybrid GNC-based nanostructures. Dots of the same color represent hybrid nanostructures made with the same excitation energy dose. The pink area represents the variation range of the fluorescence lifetime of FPSs attached on polymer dots in the absence of gold particles. (d) The simulated average Purcell factor (P) of dipoles varies as the nano-polymer distribution changes by considering different incident energy dose and resulting average thickness. (e) and (f) are simulated field intensity (at Z= 25 nm away from the bottom of the cube) of a hybrid FPS-GNC nanostructure fabricated using the energy dose of 40% D_{th} and 5% D_{th} individually. The excitation wavelength is set at 532 nm, and the incident light is polarized along X. The black dotted line depicts the FPS, and the white dotted line describes the contour of polymer.

The weighted average lifetime $(a_1\tau_1+(1-a_1)\tau_2)$ is shown in Fig. 4(c). It is represented as a function of the "average polymer thickness" defined in the Appendix E. For statistically assessing the influence of the dose, many (from 4 to 8, corresponding to the different dots in Fig. 4(c)) hybrid nanostructures have been made for each given dose. Combining the SEM and AFM analysis before FPSs attachment (see Appendix E, Fig. 12), estimated polymer 3D distribution and the average polymer thickness can be related to the levels of energy dose. Consequently, the change in the fluorescence lifetime of FPSs can be presented as a function of the average polymer thickness, as shown in Fig. 4(c) that clearly statistically reveals a trend: the lifetime decreases as the average polymer thickness decreases and tends to a stable value ~ 2ns. Fig. 4(d) shows the corresponding simulated results through the inverse of the Purcell factor, i.e. the ratio of the de-excitation rate with and without the GNC. The fluorescence

lifetime was calculated by placing dipoles at the center of FPSs at the position corresponding to the polymer distribution, as observed by SEM and AFM (see Appendix E). Fig. 4(c) and 4(d) reveal a consistent lifetime change trend, which confirms that the average polymer thickness is controlled by the incident energy dose used for fabrication of the hybrid nanosource, resulting in the control of the FPS-GNC distance and fluorescence lifetime of FPSs. As a conclusion of this section, through fittings, it turns out that, while τ_1 and τ_2 remain relatively stable, a1 is very sensitive to the polymer thickness, resulting in significant sensitivity of the resulting averaged weighted lifetime ($a_1\tau_1+(1-a_1)\tau_2$) that can be viewed as a « tunable barycenter » in the continuous sum of lifetimes in Eq. 1.

C. Further Discussion about the contributing molecules within the FPS

From Fig. 4(c) and 4(d), a maximum Purcell factor can be estimated at 3.1 for smallest polymer thickness, which is a rather low factor. Because of FPS' size, even is the polymer thickness is negligible, a large proportion of molecules within the FPS are still too far away from GNC, and the proportion of the unaffected/less affected molecule cannot go to zero. As a result, (1-a1) always >0. This point is illustrated by Fig. 4(e) and 4(f) in terms of near-field excitation. Two hybrid nanosources were considered: one fabricated with a 40% Dth dose [Fig. 4(e)], polymer thickness = 21.6 nm, (see Appendix E, Table 1) and one fabricated with a 5% Dth [Fig. 4(f)], polymer thickness = 2 nm (see Appendix E Table 1). For simplicity, both hybrid nanosources present a single FPS. The intensity map at Z=25 nm (λ=532 nm) was calculated by FDTD using an incident X-polarized plane wave propagating along Z. The spatial distribution of the intensity reveals the two families of molecules in terms of excitation: in Fig. 4(e), there is a fewer proportion of dyes inside polystyrene sphere that are coupled to the localized field of the GNC ("close"). Even if this near-field map represents the excitation (rather than the deexcitation to the LDOS), it illustrates that the contribution of plasmon-coupled molecules to the average lifetime/Purcell factor of the whole system is weak; most of the molecules whose lifetime play the main role in the whole system are unaffected from GNC ("far"). In Fig. 4(f), a bigger proportion of dyes are coupled to the localized plasmonic near-field and their contribution to lifetime decrease becomes significant. This is consistent with the double exponential fitting results in Fig. 4(b). The above discussions can also explain why when the polymer thickness decreases to the smallest, the weighted lifetime/average Purcell factor does not continue declining but tends to stabilize in Fig. 4(c)/(d).

D. Use of semiconductor colloidal quantum dots as nano-emitters

In order to address the above issue, another approach was investigated: semiconductor colloidal quantum dots were immobilized on a functionalized nanopolymer surface in the close vicinity of a single gold nanocube. Compared to FPS, they can be considered as point-like emitters. After step 1 of fabrication (illustrated in Fig. 1(d)) the hybrid GNC was immersed in a colloidal solution of negatively charged CdSe/ZnS red QDs (with carboxylic acid as reactive group, bought from Mesolight), with emission wavelength at 623 nm and diameter ≈ 12 nm (Fig. 8(c)(d), Appendix B). The obtained results, presented in Fig. 5(a), show a precise and selective attachment of QDs on the two corners of the gold nanocube where the functionalized polymer was printed by the plasmon-induced polymerization: Fig. 5(a) is the AFM image of a hybrid polymer/GNC/QDs obtained with a 40 % Dth energy used for fabrication (step 1). It clearly shows QDs attached at the surface of the integrated polymer lobes. More data with different energy doses can be found in Appendix C (Fig. 10).

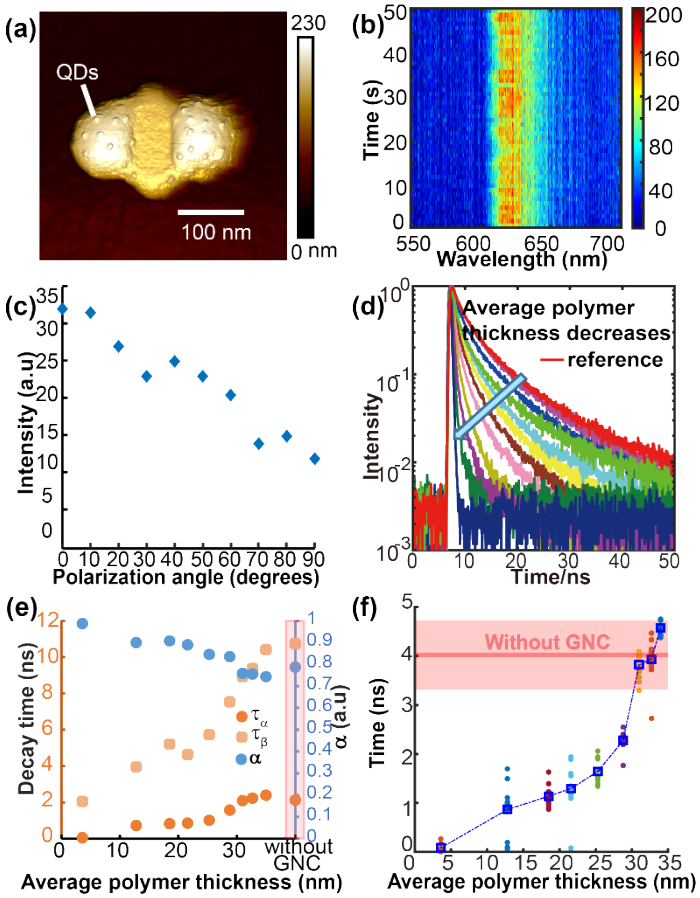

Fig 5. Use of the smart polymer for coupling spherical CdSe/ZnS quantum dots with gold nanocubes. (a) AFM image of a hybrid nanosource made with an energy dose of 40 % D_{th}. Attached QDs resulting from step 2 of fabrication are clearly visible. (b) The spectrum time trace, signal collected during continuous 50s. (c) Polarization sensitivity of the hybrid nanosource. (d). Measured lifetime for different hybrid nanosources having different polymer thicknesses. The red curve represents a reference lifetime decay of QDs attached on a polymer dot without GNC nearby. (e) Double-exponential fitting results: evolution of fast and slow decay components τ_α, τ_β and coefficient α of fast component as a function of the average polymer thickness. (f) Weighted lifetime as a function of the average polymer thickness that depends on the fabrication condition (% D_{th} energy used for near-field photo polymerization in step 1).

Fig. 5(b) shows a typical PL spectrum centered at λ=620 nm collected in the far field for 50 s (excitation at 405 nm). As for the FPS-based hybrid sources, the active medium is anisotropic, making the sources sensitive to the incident polarization: Fig. 5(c) shows the PL intensity as a function of the polarization direction of the excitation at 405 nm (the definition of this direction is the same as for Fig. 3(c)).

QDs generally have multi-exponential decay dynamics, which are due to their surface defects, surface ligands, inhomogeneities of ensemble sample or other characteristics.[44–46] Unlike in the situation with FPSs, the reference lifetime from QDs attached on the polymer dot without GNC nearby can be fitted well by double-exponential decay (Fig. 15(a), Appendix G). The short-time component and long-time component come from two different decay pathways [47]. Without QDs, these both lifetime represents a reference that is intrinsic to the semiconducting nanocrystal

With the presence of GNC, QDs' decay is influenced by the Purcell effect depending on their relative positions to GNC. The lifetime of QDs can still be fitted by double exponential functions (Fig. 15(b), Appendix G). Then the normalized intensity can be presented as

$$I(t) = \alpha \exp(-t/\tau_\alpha) + (1-\alpha)\exp(-t/\tau_\beta), \quad (3)$$

where the τ_α is the fast decay and τ_β is the slow decay. α decribes the contribution of τ_α. Fig. 5(d) shows a typical lifetime measurement of different hybrid nanosources fabricated with different energy doses ranging from 10% to 90% of D_{th}. From Fig. 5(d), the curves are fitted by double-exponential decay, using equation (3) and the fitting results are shown in Fig. 5(e).

The origin of this double-exponential decay is different from it is in Eq. (2): In Eq. (3), it results from the intrinsic properties of the QDs [44-47] while it corresponds to two families of molecules in Eq. (2) ("far" and "close" molecules). Due to the small size of QDs, all the QDs are affected in the same way by the presence of the GNC (Fig. 13, Appendix E). As the result, both lifetimes are sensitive to the polymer thickness, as shown in Fig. 5(e).

Fig. 5(f) shows the weighted average lifetime ($\alpha\tau_\alpha+(1-\alpha)\tau_\beta$) for different polymer thicknesses. Again, for each dose, many similar structures (from 6 to 9) were fabricated to get a statistical trend. From Fig. 5(d) and 5(f), it turns out that the weighted average lifetime decreases with the dose, as a result of the decrease of the average distance between quantum nano-emitters and GNC. Fig. 5(e) shows the fitted values τ_α, τ_β and α, as a function of the average polymer thickness. Compared to Fig. 4(b), Fig. 5(e) reveals different features of interest. In Fig. 4(b), we saw that both decay components are almost stable, and a_1 increases obviously as the polymer thickness decreases, mainly revealing the increase of the proportion of molecules that are influenced by the GNC and a displacement of the barycenter in Eq. 1. In Fig. 5(e), the components are both affected: τ_α and τ_β decrease together as the average polymer thickness gets smaller. (It is actually impossible to keep τ_α and τ_β stable, see Fig. 15 (c)) Meantime, coefficient α presents a weak increase (0.8 to 1), which is still much tiny compared to the situation of FPS-attached hybrid GNC (in Fig. 4(b), a_1 varies from 0.9 to 0.1). There are two possible explanations for this. First, α not only represents the intrinsic ratio between the two decay pathways but also includes the weak increase of the proportion of QDs influenced by GNC as the polymer thicknesses decreases. Second, the short-time component of QDs already plays the major role in free space, the change of it cannot be distinguished as the change of the long-time component because of the resolution limitation of the set-up. For FPSs, instead, the variation of weighted average lifetimes is mainly due to a_1. In addition, according to Fig. 5F, quite different from Fig. 4(c), the maximum Purcell factor in the situation of attached QDs can get larger than 10. This is because, due to their small size, at a small polymer thickness, quantum dots may be strongly affected by the Purcell effect, and no quantum dots can escape from the influence of GNC.

4. CONCLUSION

The use of a smart photopolymer has been leading to a new kind of plasmonic hybrid nanosources where different types of nano-emitters can be integrated on demand at predesigned sites of the metal nanostructures. The cleverness of the polymer makes possible the selection of the site through local preliminary plasmon excitation resulting in a 3D spatial memory. In particular, it is possible to control the average distance between the metal nanostructure and the

emitter to be attached. This latter is recognized by the polymer through charge affinity, leading to its selective controlled attachment.

Compared to Ref. 33, many advantages can be stressed. First, we can achieve a wider variety of emitters. While the integration of emitters within the initial acrylate-type liquid formulation is delicate in terms of phase separation and photochemical effects [48], the new approach reported here allows any negatively-charged emitters or particles to attach on the surface of polymer lobes with the help of electrostatic forces. In the future, this approach will open up many routes. For example, even negatively charged nanodiamonds permitting single photon emission [49] could be selectively attached. Second, the main novelty lies on the fact we remain the advantages of our previous method, which can place emitters close to plasmonic structures with anisotropic distribution and further improve it with more possibilities. By placing emitters on the surface of the polymer, the thickness of polymer is also the distance between emitters and plasmonic particles, instead of letting the emitters randomly dispersed inside the whole volume of the polymer lobes. The control of this distance has been leading to an actual lifetime engineering. In order to comment further on this point, let us use the spherical coordinates (ϕ, θ, ρ) of the emitter to be localized. We can control ϕ, θ using the method introduced in Ref. 33. We now control ρ with our new approach of functionalized photopolymer.

Finally, the surface attachment method is likely to avoid bad influence from the laser during polymerization, which may damage the emitters or introduce other effects such as light force, and two-photon absorption, etc. These effects are currently being studied by our team.

This approach will be used for fabricating single-photon hybrid nanosources [33] and precisely integrating different kinds of QDs through a multistep process [34], which will be opening new avenues for advanced integrated nanosources based on weak and strong coupling, among which multicolor nano lasers [34,50] that may be controlled by light polarization. Besides, as we demonstrated in Ref. 33, a tunable emitter selection is possible by rotating the incident polarization, through the concept of polarization-dependent spatial overlap integral (overlap between the exciting near-field and the emitters). However, in ref. 33, the excitation was in the blue, which is suitable for emitter excitation but not plasmon excitation. By integrating emitters that efficiently get excited at 780 nm wavelength through either one or two-photon absorption, we would take advantage of the plasmonic hot spot for both integrating and exciting them in the future.

APPENDIX A: PROCESS OF FBRICATION

The separation distance between each GNC is controlled bigger than 500nm by adjusting the concentration of GNCs in solution, to avoid the influence from each other in the following experiments including 2-photon polymerization and emission measurement.

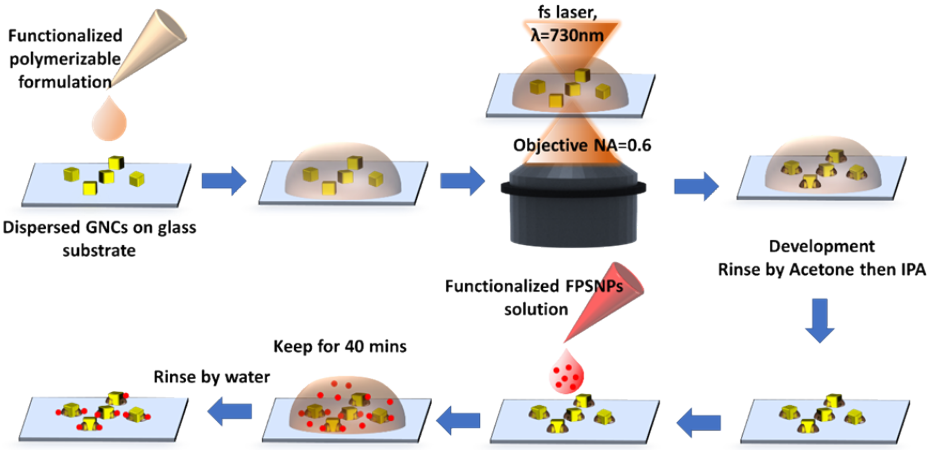

Fig. 6. The process steps for fabricating hybrid FPSs-attached cubes.

Fig. 6 illustrates the whole steps for preparing hybrid FPSs-attached cubes. And Fig. 7 gives out the optical set-up used for doing 2-pjoton polymerization on each single GNC. The position of focused laser spot and GNCs are observed by a CCD camera and makes it possible to aim the laser spot at each isolated GNC. Plasmon-triggered 2-photon polymerization process

The GNCs are dispersed on a glass substrate with a separation distance between each other bigger than 500nm. A drop of the functionalized photosensitive formulation is then deposited on the pre-identified GNCs sample. Each GNC of consistent size and good shape is exposed one by one using a focused femtosecond laser of 730nm by an objective lens (N. A=0.6) (Fig. 7). During polymerization, the exposure time is kept at 1/15 s. The exposure laser energy dose is set below than the polymerization threshold and is defined as the percentage of threshold dose (typical incident dose Din =40% Dth). The polarization direction of curing laser is along the diagonal of the GNCs.

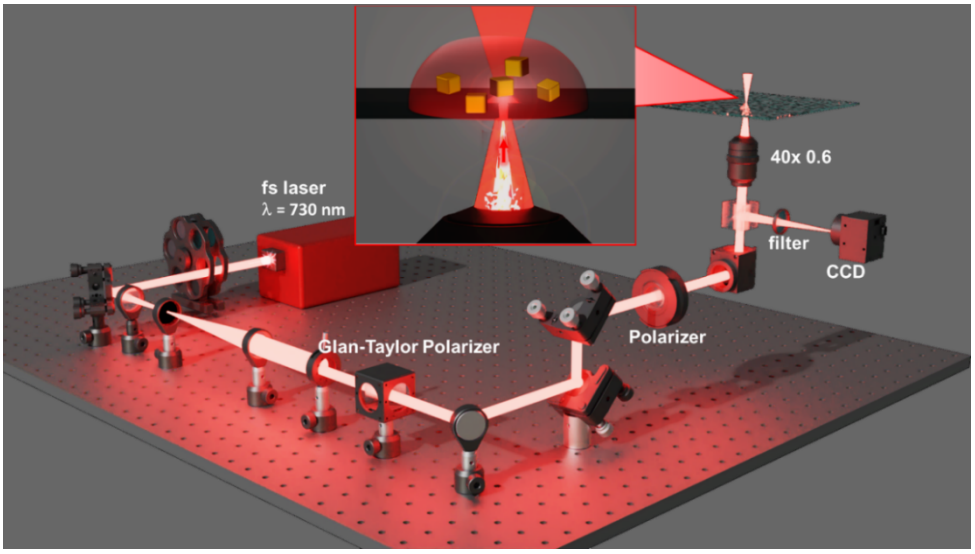

Fig. 7 Optical configuration to carry out two-photon polymerization.

APPENDIX B: SIZE OF POLYSTYRENE FLUORESCENT PARTICLES AND QUANTUMN DOTS

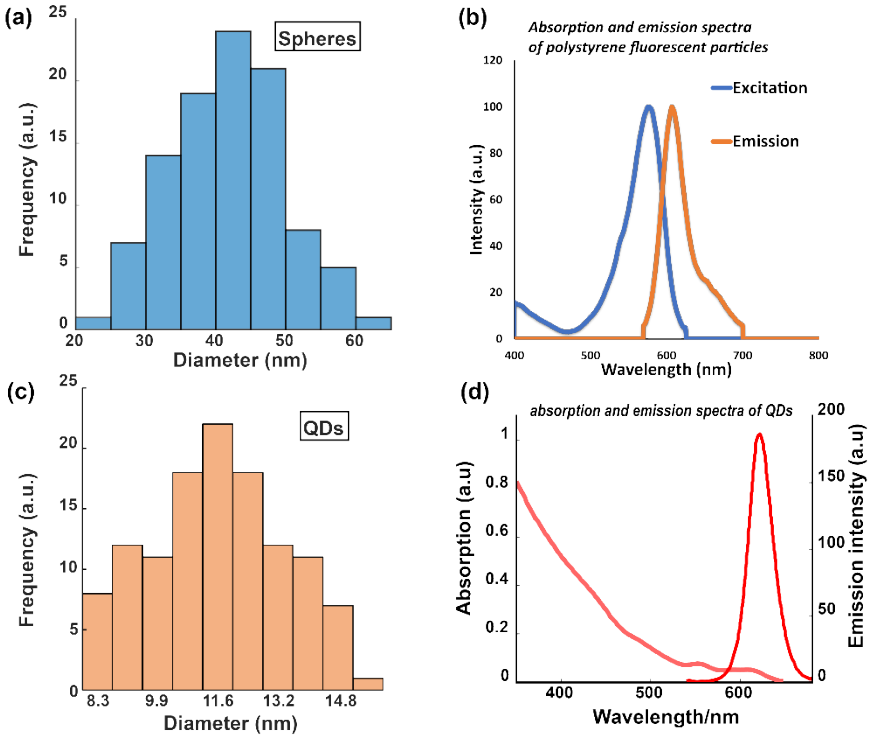

Fig. 8 (a) Diameter distribution histogram of the polystyrene fluorescent spheres (b) Excitation and emission spectra of polystyrene spheres measure by UV-visible Cary 100 spectrometer and Fluorescence Spectrophotometer separately. (c) Diameter distribution histogram of the QDs. The QDs are deposited on glass substrate and then after coating of a conducting layer, the QDs 'sizes are measured under SEM. Due to the existence of the conductive layer, the size of the measured QD is several nanometers larger than the real size of QDs. (d) The absorption and emission spectra of the red QDs in toluene.

From Fig. 8(a), the average diameter of this kind of polystyrene fluorescent sphere is around 42.5nm. Different sizes of polystyrene spheres will change the related distance between their containing fluorescent dye molecules and the GNC, which will lead to errors in the fluorescence lifetime measurement. When the number of attached polystyrene spheres is relatively large, since the measured fluorescence lifetime is a statistical average, the influence of the size difference of polystyrene spheres on the result can be ignored. However, when the hybrid GNC is fabricated by low dose, the number of attached polystyrene spheres is limited, the size difference of the fluorescent spheres becomes non-negligible. That can explain why the measured lifetime in the situation of smallest average thickness is bigger than the second smallest situation in Fig. 4b of the article.

These Fluorescent FluoSpheres beads whose average diameter are around 42nm with the dyes filling the full volume of the beads and contain 3500 fluorescein equivalents per microsphere according to the handbook from Thermofisher.

APPENDIX C: MORE EXAMPLES OF HYBRID NANOCUBES

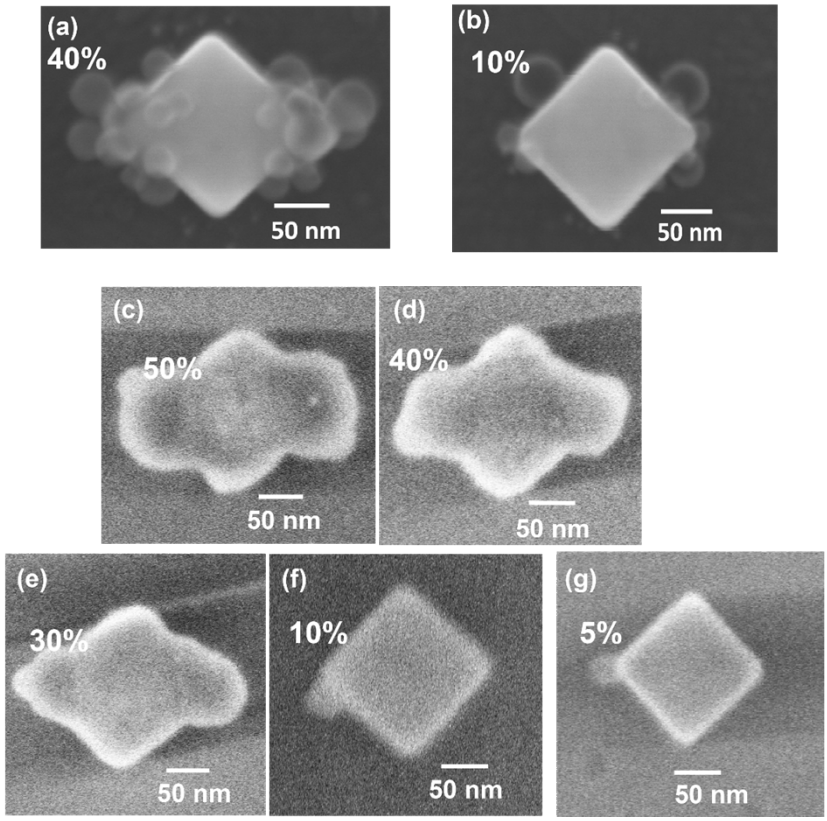

Fig. 9 More examples of hybrid FPSs-attached gold nanocubes. (a) and (b) SEM images of the hybrid FPSs-attached nanocubes fabricating using 40% D_{th} and 10% D_{th}, and the residence time of FPS solution is 40 mins. 10kV voltage is used for SEM observation. (c) (d) (e) (f) (g) fabricated using 50% D_{th} 40% D_{th}, 30% D_{th} 10% D_{th} 5%D_{th} separately, and the immersion time of the sample in the FPS solution decreased to 10 mins. 1kV voltage is used for SEM observation

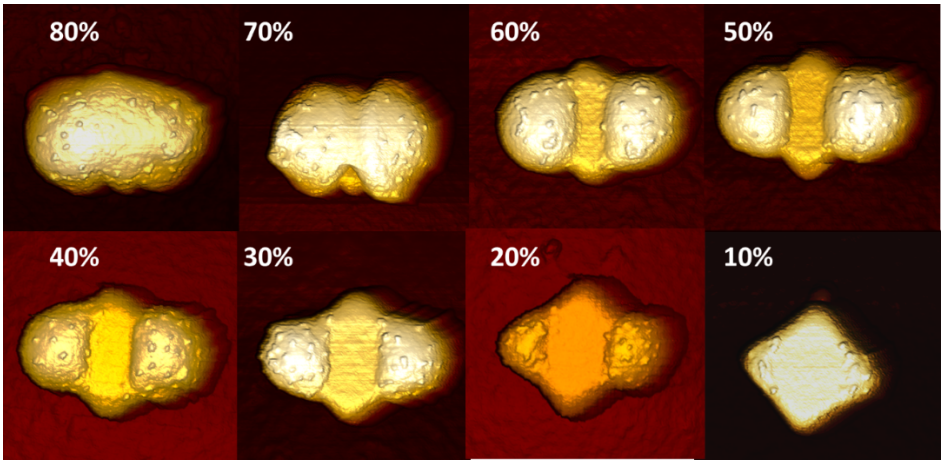

Fig. 10 AFM images of some hybrid GNC with attached QDs, fabricated using incident doses from 80% decreasing to 10% of Dth (step 1).

APPENDIX D: POLARIZATION SENSITIVITY OF THE EMISSION INTENSITY

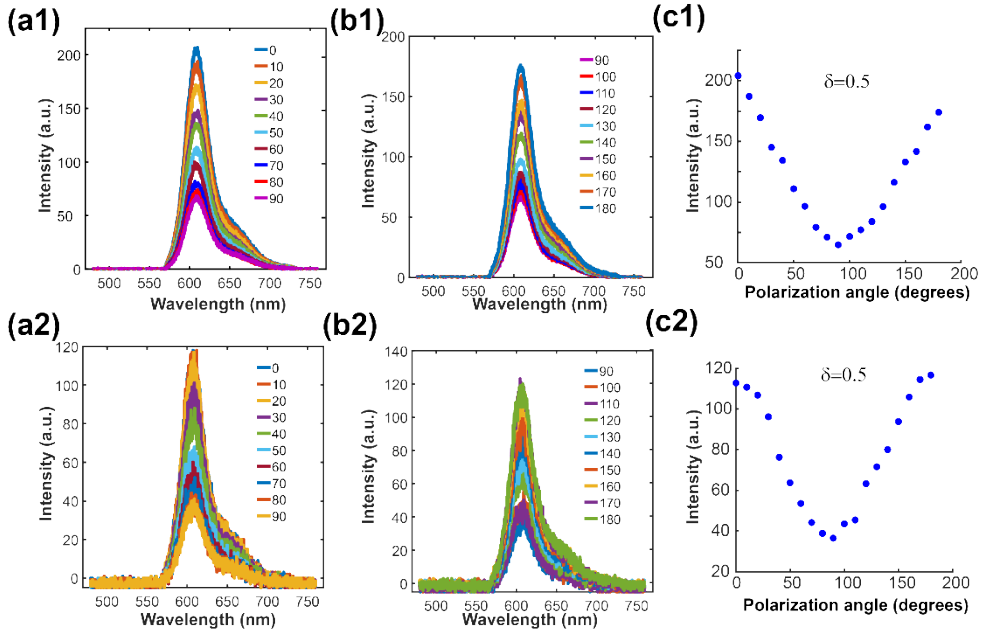

Fig. 11 Emission spectra from two hybrid FPSs-attached nanocubes fabricated using same parameters, their exposure dose is 40% D_{th}. (a1) and (b1) are the emission spectra from the first hybrid FPSs-attached nanocube when the polarization angle of the laser used for exciting varies from 0 degrees to 90 degrees and 90 degrees to 180 degrees separately. (c1) is the emission peak intensity changing trend. And (a2) (b2) (c2) are the results from the second hybrid FPSs-attached nanocube.

APPENDIX E: 3D POLYMER CHARACTERIZATION AND DEFINITION OF THE AVERAGE POLYMER THICKNESS

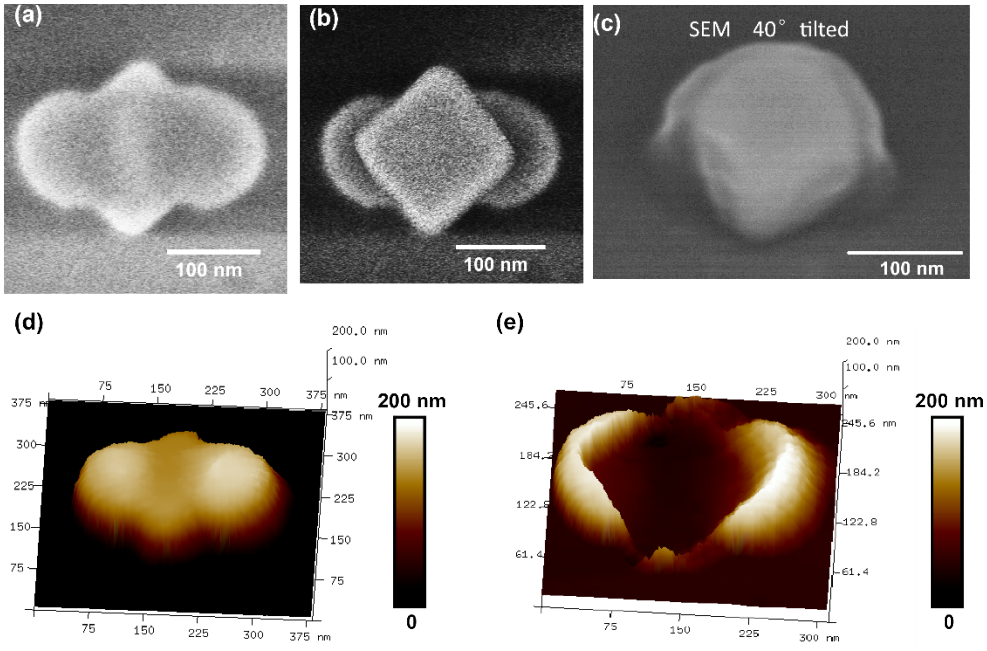

Fig. 12 (a)SEM image of a hybrid nanocube without attaching any QDs/polystyrenes (fabricated using 50% Dth) (b) Mixed image, the original SEM image of the cube before exposure is superimposed to (a). (c) 40-degree tilted SEM

image. (d) 3D height image measured by AFM of the same hybrid nanocube of (a). (d) 3D height image subtracted by the original cube's height profile from (c), demonstrating the 3D polymer distribution.

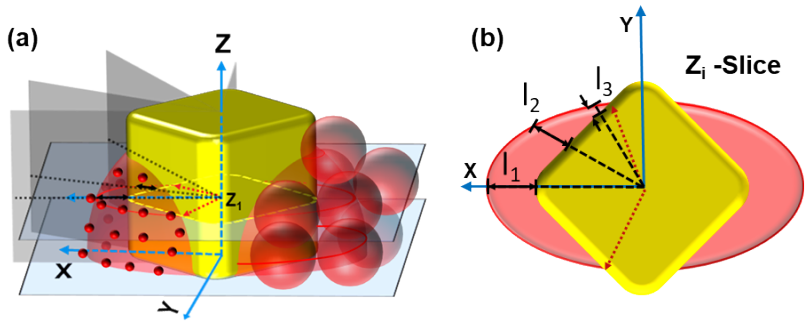

Fig. 13. Average polymer thickness definition and assessment. (a) The whole hybrid cube-polymer structure is cut in the Z direction to get 20 slices of the cross-section. For each z-slice, a quadrant is sliced into n parts on average according to angle, and the intersection of the corresponding rays and the polymer profile is averaged to obtain the average elongation of the polymer under this Z slice. Finally, the polymer thickness of all slices in the z-direction is averaged to get the average polymer thickness. (b) shows the polymer elongations (l_1, l_2, l_3) obtained by the three tangents when a quadrant is divided into 3 sections in the z1-slice, then the average value of the three elongation rates of the polymer thickness of this slice.

For Z_i-slice, If the polymer thickness in the third quadrant is sampled at 30-degree intervals shown in Fig. 13(b), three polymer thickness l_1, l_2, l_3 are obtained. Then the average polymer thickness on Z_i-slice is $(l_1+l_2+l_3)/3$. For each Z_i-slice, keep sampling at 30-degree intervals, and the number of l obtained will vary with the change of the polymer distribution of each slice. Finally, the average of all the obtained l is taken as the average polymer thickness.

Table 1. Calculated average polymer thickness, when using different dose in percentage of Dth

Percentage of Dth (%)	Average polymer thickness (nm)
5	2
10	3.6
20	12.8
30	18.5
40	21.6
50	25.3
60	28.8
70	31.0
80	32.7
90	34

APPENDIX F: FLUORESCENCE SIGNAL AND LIFETIME MEASUREMENT

A. Optical set-up

For fluorescence intensity measurement, every single FPSs-attached hybrid polymer-cube is excited using 532nm (CW laser, OBIS 532nm) focused by an objective lens of 40 x 0.6, and its fluorescence signal is collected by the same objective, after fitting by a band-pass filter (FF01-650/150-25), it is analyzed by a spectrometer. A half-wave plate is used to change the

polarization direction of linearly polarized laser and after each polarization rotation, use another polarizer to check the polarization direction, and fine-tune the laser output light power to ensure that the power reaching the sample surface remains the same (detected before objective lens, laser power is set to 10 μw). For lifetime measurement, a pulsed laser (Picoquant D-TA-530B) connected with an extra driver box (PDL 800-B), whose repetition frequency is set at 10MHz is used. The laser beam is focused on the scanning sample hold stage by an objective lens of 100 x 0.95. The laser power detected before objective lens is about 0.5 □w. For each hybrid FPSPNs-attached polymer-cube, its fluorescence is collected by reflection, and then after passing through a band-pass filter (FF01-650/150-25), the collected light is directed by a fiber towards an APD (Picoquant PMA- 182). The signal is sent to the stand-alone TCSPC Module (TimeHarp-300), which is linked to the laser driver.

B. Purcell factor simulation

The Purcell factor is calculated by FDTD. For each incident light dose, the corresponding 3D polymer is constructed as a model with a refractive index of 1.5. And set the diameter of the polystyrene sphere to 50mm. For each case, the hybrid polymer cube is cut into N slices in the z direction, each Z_i-slice has a specific polymer contour at the z position, as shown in Fig. 13. The FPSs are distributed along the contour of the polymer. To calculate, we only chose several FPSs along the contour at Z_i. For each nanosphere, calculate the Purcell factor of the ideal dipole at the center of the nanosphere, and finally average these results to obtain the average Purcell factor of this z-slice, see Equation (F-1)

$$PF_i = \frac{1}{N_i}\sum_{k=1}^{N_i} PF_k \tag{F-1}$$

Where N_i is the sampling number of FPSs on Z_i slice.

The FSNPs are assumed uniformly distributed on the surface of polymer, then for each Z_i-slice, the number of attached FSNPs depends on the length of the polymer contour line.

$$PF_{total} = \left(\sum_{i=1}^{i=N} C_i \bullet PF_i\right) / \left(\sum_{i=1}^{i=N} C_i\right) \tag{F-2}$$

Where C_i is the length of polymer contour line of Z_i-slice, and N is the number of slices in z-direction.

By this way, the obtained PF_{total} is worked as the average Purcell factor in the case of a hybrid FPSs-attached polymer-cube fabricated by a certain dose.

For example, of 20% Dth, the polymer volume is cut into 2 slices in the z direction. For slice1, 3 positions of fluorescent spheres are calculated. For every position, we calculated the Purcell factor of an orientation-averaged dipole placed in the center of sphere. And the boundary length of the polymer of this Z_1-slize is around 48.7nm. For Z_2-slice, because the boundary length of polymer is much smaller than diameter of sphere, we only calculate the Purcell factor at one position. Finally, an average Purcell factor ~2.17 was obtained according to Eq. F-2

APPENDIX G: MULTI-EXPONENTIAL DECAY FITTING OF THE LIFETIME OF FPS AND QD IN FREE SPACE

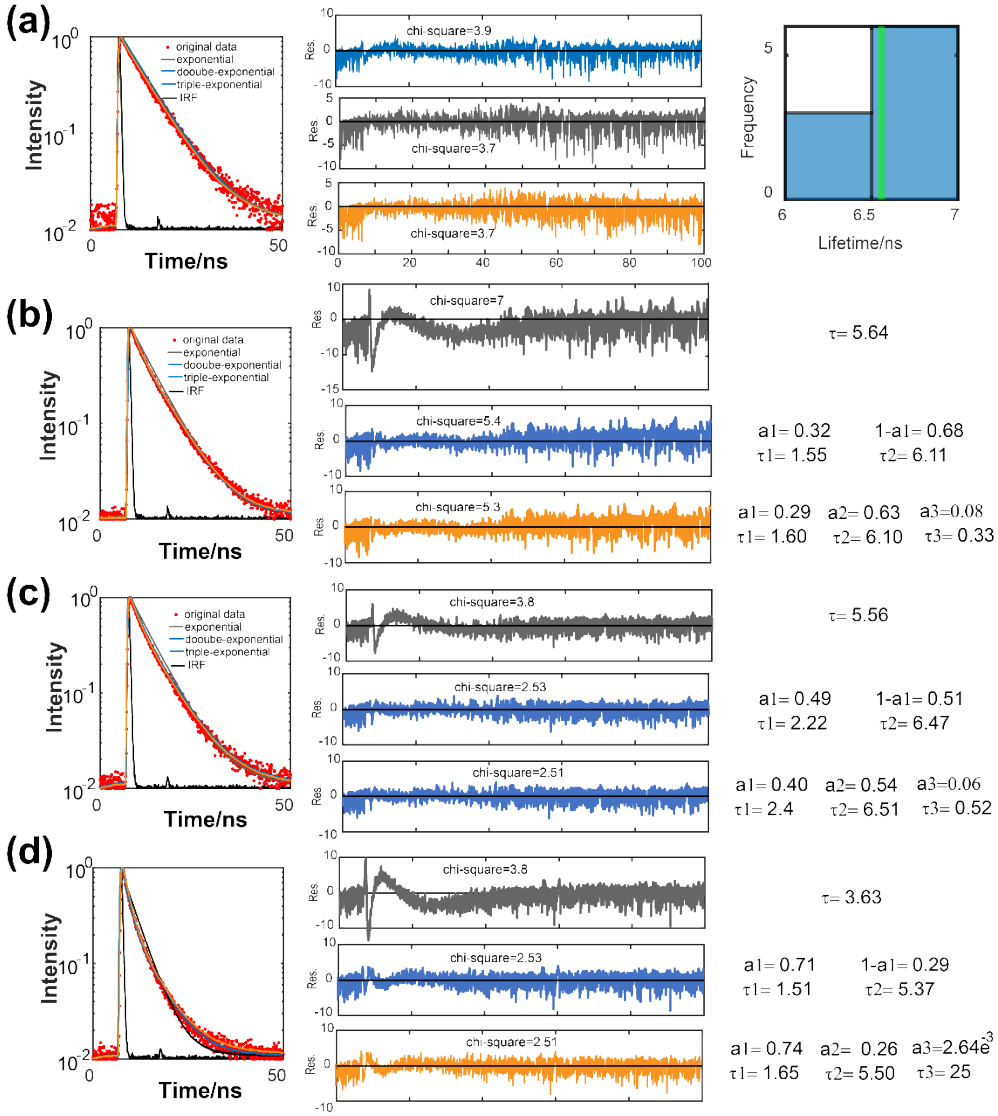

Fig. 14 (a) The first row shows an example of the lifetime from FPSs attached on pure polymer dot without Au nanocube nearby. Two kinds of fitting, single-exponential fitting (grey line) and double-exponential fitting (blue line), triple-exponential fitting (orange line) are used here. From the fitting results, the single exponential function can already achieve good fitting result. The far-right image shows the histogram of FPSs' lifetime under single exponential fitting, and the green line represents the average value. For comparison (b) (c) and (d) show three examples of the lifetime from FPSs attached on polymer lobes of GNC.

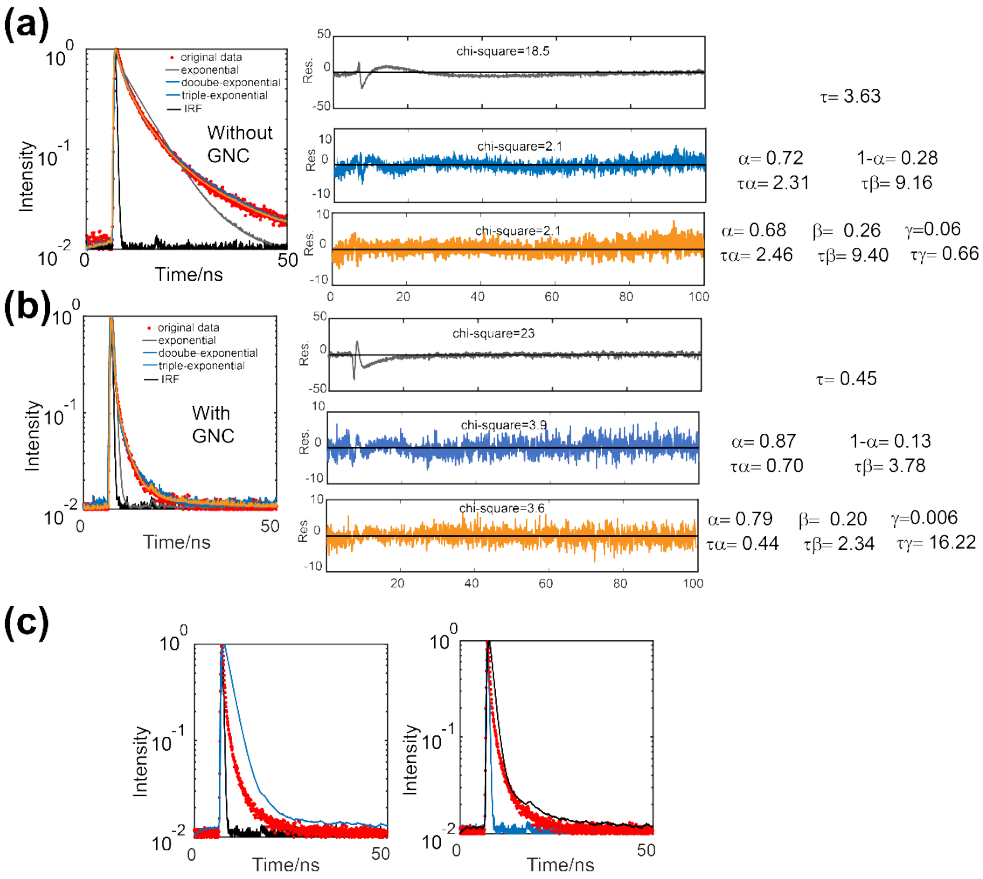

Fig. 15 Example of the lifetime from QDs attached on pure polymer dot without Au nanocube nearby (a) and with Au nanocube nearby (b). Single-exponential function is not enough to get a good fitting result while double/triple-exponential function can get a better fit. (c) Two failed attempts. By limiting the value range of τ_a (2-3), τ_β (9-10), and τ_α (1-3), τ_b (8-10) to attempt to use similar τ_α, τ_b in (a) to fit the decay curve.

APPENDIX H: NUMBER OF ATTACHED EMITTERS

In Ref. 36, the original principle of this chemically attached method has been described. In this article, gold nanoparticles (diameter~ 50nm) were attached to the smart photopolymer. The control of the surface density (and thus the number) of gold nanoparticles has already been studied. The gold nanoparticles have same size as the fluorescent spheres used in our current manuscript. We expect that their density changes with the immersion time following the same law.

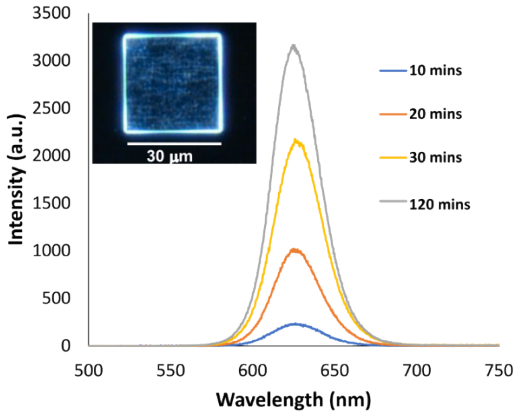

Fig. 16 Fluorescence intensity from QDs attached on 2D flat functionalized polymer structure (see inset) with respect to the immersion time (mins). The excitation laser is 405 nm with a power of 2µm, collection time is kept as 0.1s. The left top small image (inset) is the dark-field image of the 2D flat polymer square.

As far as the QDs are concerned, Fig.16 shows the fluorescence intensity from QDs attached on a micrometer sized functionalized flat polymer structure. Different times of immersion were used. Considering the fixed size of the polymer area, this Fig. 16 clearly shows that the intensity (and thus the related number of attached QDs) strongly depends on the immersion time.

Funding. PRONANO project co-funded by FEDER and the region Grand Est. Q-LED project funded by FEDER and UTT.

Acknowledgments. D. Ge thanks the CSC for funding support. Fabrication and characterization were mostly done thanks to the Nano'mat Platform, supported by the Ministère de l'Enseignement Supérieur et de la Recherche, the Région Grand Est (Pronano project), the Conseil Général de l'Aube, and FEDER (Pronano and Q-LED projects) funds from the European Community. This work has been made within the framework of the Graduate School NANO-PHOT (École Universitaire de Recherche, contract ANR-18-EURE-0013). The manuscript was written through contributions of all authors. All authors have given approval to the final version of the manuscript.

Disclosures. The authors declare no conflicts of interest.

Data availability. Data underlying the results presented in this paper are not publicly available at this time but may be obtained from the authors upon reasonable request.

Reference

1. F. Vetrone, R. Naccache, A. Zamarrón, A. Juarranz de la Fuente, F. Sanz-Rodríguez, L. Martinez Maestro, E. Martin Rodriguez, D. Jaque, J. Garcia Sole, and J. A. Capobianco, "Temperature sensing using fluorescent nanothermometers," ACS nano **4**, 3254–3258 (2010).
2. J.-H. Kim, S. Aghaeimeibodi, C. J. K. Richardson, R. P. Leavitt, D. Englund, and E. Waks, "Hybrid Integration of Solid-State Quantum Emitters on a Silicon Photonic Chip," Nano Lett. **17**, 7394–7400 (2017).
3. X. Feng, Y. Li, X. He, H. Liu, Z. Zhao, R. T. K. Kwok, M. R. J. Elsegood, J. W. Y. Lam, and B. Z. Tang, "A Substitution-Dependent Light-Up Fluorescence Probe for Selectively Detecting Fe3+ Ions and Its Cell Imaging Application," Adv. Funct. Mater. **28**, 1802833 (2018).
4. T. B. Hoang, G. M. Akselrod, C. Argyropoulos, J. Huang, D. R. Smith, and M. H. Mikkelsen, "Ultrafast spontaneous emission source using plasmonic nanoantennas," Nat. Commun. **6**, 7788 (2015).
5. G. M. Akselrod, C. Argyropoulos, T. B. Hoang, C. Ciracì, C. Fang, J. Huang, D. R. Smith, and M. H. Mikkelsen, "Probing the mechanisms of large Purcell enhancement in plasmonic nanoantennas," Nature Photon. **8**, 835–840 (2014).
6. Y. Luo, E. D. Ahmadi, K. Shayan, Y. Ma, K. S. Mistry, C. Zhang, J. Hone, J. L. Blackburn, and S. Strauf, "Purcell-enhanced quantum yield from carbon nanotube excitons coupled to plasmonic nanocavities," Nat. Commun. **8**, 1413 (2017).
7. H. Aouani, O. Mahboub, E. Devaux, H. Rigneault, T. W. Ebbesen, and J. Wenger, "Plasmonic Antennas for Directional Sorting of Fluorescence Emission," Nano Lett. **11**, 2400–2406 (2011).
8. P. Anger, P. Bharadwaj, and L. Novotny, "Enhancement and Quenching of Single-Molecule Fluorescence," Phys. Rev. Lett. **96**, 113002 (2006).

9. H. Leng, B. Szychowski, M.-C. Daniel, and M. Pelton, "Strong coupling and induced transparency at room temperature with single quantum dots and gap plasmons," Nat Commun **9**, 4012 (2018).
10. A. Kinkhabwala, Z. Yu, S. Fan, Y. Avlasevich, K. Müllen, and W. E. Moerner, "Large single-molecule fluorescence enhancements produced by a bowtie nanoantenna," Nature Photon. **3**, 654–657 (2009).
11. S. Khatua, P. M. R. Paulo, H. Yuan, A. Gupta, P. Zijlstra, and M. Orrit, "Resonant Plasmonic Enhancement of Single-Molecule Fluorescence by Individual Gold Nanorods," ACS Nano **8**, 4440–4449 (2014).
12. K. J. Russell, T.-L. Liu, S. Cui, and E. L. Hu, "Large spontaneous emission enhancement in plasmonic nanocavities," Nature Photon. **6**, 459–462 (2012).
13. R. Chikkaraddy, B. de Nijs, F. Benz, S. J. Barrow, O. A. Scherman, E. Rosta, A. Demetriadou, P. Fox, O. Hess, and J. J. Baumberg, "Single-molecule strong coupling at room temperature in plasmonic nanocavities," Nature **535**, 127–130 (2016).
14. T. B. Hoang, G. M. Akselrod, and M. H. Mikkelsen, "Ultrafast Room-Temperature Single Photon Emission from Quantum Dots Coupled to Plasmonic Nanocavities," Nano Lett. **16**, 270–275 (2016).
15. T. Ming, L. Zhao, Z. Yang, H. Chen, L. Sun, J. Wang, and C. Yan, "Strong polarization dependence of plasmon-enhanced fluorescence on single gold nanorods," Nano Letters **9**, 3896–3903 (2009).
16. S.-Y. Liu, L. Huang, J.-F. Li, C. Wang, Q. Li, H.-X. Xu, H.-L. Guo, Z.-M. Meng, Z. Shi, and Z.-Y. Li, "Simultaneous Excitation and Emission Enhancement of Fluorescence Assisted by Double Plasmon Modes of Gold Nanorods," J. Phys. Chem. C **117**, 10636–10642 (2013).
17. A. W. Schell, P. Engel, J. F. M. Werra, C. Wolff, K. Busch, and O. Benson, "Scanning Single Quantum Emitter Fluorescence Lifetime Imaging: Quantitative Analysis of the Local Density of Photonic States," Nano Lett. **14**, 2623–2627 (2014).
18. H. Groß, J. M. Hamm, T. Tufarelli, O. Hess, and B. Hecht, "Near-field strong coupling of single quantum dots," Sci. Adv. **4**, eaar4906 (n.d.).
19. M. P. Busson, B. Rolly, B. Stout, N. Bonod, and S. Bidault, "Accelerated single photon emission from dye molecule-driven nanoantennas assembled on DNA," Nat. Commun. **3**, 1–6 (2012).
20. X. Lan, X. Zhou, L. A. McCarthy, A. O. Govorov, Y. Liu, and S. Link, "DNA-Enabled Chiral Gold Nanoparticle–Chromophore Hybrid Structure with Resonant Plasmon–Exciton Coupling Gives Unusual and Strong Circular Dichroism," J. Am. Chem. Soc. **141**, 19336–19341 (2019).
21. A. T. M. Yeşilyurt and J.-S. Huang, "Emission Manipulation by DNA Origami-Assisted Plasmonic Nanoantennas," Adv. Opt. Mater. **9**, 2100848 (2021).
22. M. Loretan, I. Domljanovic, M. Lakatos, C. Rüegg, and G. P. Acuna, "DNA Origami as Emerging Technology for the Engineering of Fluorescent and Plasmonic-Based Biosensors," Materials **13**, 2185 (2020).
23. K. Hübner, M. Pilo-Pais, F. Selbach, T. Liedl, P. Tinnefeld, F. D. Stefani, and G. P. Acuna, "Directing Single-Molecule Emission with DNA Origami-Assembled Optical Antennas," Nano Lett. **19**, 6629–6634 (2019).
24. R. Chikkaraddy, V. A. Turek, N. Kongsuwan, F. Benz, C. Carnegie, T. van de Goor, B. de Nijs, A. Demetriadou, O. Hess, U. F. Keyser, and J. J. Baumberg, "Mapping Nanoscale Hotspots with Single-Molecule Emitters Assembled into Plasmonic Nanocavities Using DNA Origami," Nano Lett. **18**, 405–411 (2018).
25. H. Zhang, M. Li, K. Wang, Y. Tian, J.-S. Chen, K. T. Fountaine, D. DiMarzio, M. Liu, M. Cotlet, and O. Gang, "Polarized Single-Particle Quantum Dot Emitters through Programmable Cluster Assembly," ACS Nano **14**, 1369–1378 (2020).
26. G. P. Acuna, F. M. Möller, P. Holzmeister, S. Beater, B. Lalkens, and P. Tinnefeld, "Fluorescence Enhancement at Docking Sites of DNA-Directed Self-Assembled Nanoantennas," Science **338**, 506–510 (2012).
27. J. Heintz, N. Markešević, E. Y. Gayet, N. Bonod, and S. Bidault, "Few-Molecule Strong Coupling with Dimers of Plasmonic Nanoparticles Assembled on DNA," ACS Nano **15**, 14732–14743 (2021).
28. C. Shen, X. Lan, X. Lu, T. A. Meyer, W. Ni, Y. Ke, and Q. Wang, "Site-Specific Surface Functionalization of Gold Nanorods Using DNA Origami Clamps," J. Am. Chem. Soc. **138**, 1764–1767 (2016).
29. F. Wang, S. Cheng, Z. Bao, and J. Wang, "Anisotropic Overgrowth of Metal Heterostructures Induced by a Site-Selective Silica Coating," Adv. Opt. Mater. **52**, 10344–10348 (2013).
30. I. Tijunelyte, I. Kherbouche, S. Gam-Derouich, M. Nguyen, N. Lidgi-Guigui, M. L. de la Chapelle, A. Lamouri, G. Lévi, J. Aubard, A. Chevillot-Biraud, C. Mangeney, and N. Felidj, "Multi-functionalization of lithographically designed gold nanodisks by plasmon-mediated reduction of aryl diazonium salts," Nanoscale Horiz. **3**, 53–57 (2017).
31. V.-Q. Nguyen, Y. Ai, P. Martin, and J.-C. Lacroix, "Plasmon-Induced Nanolocalized Reduction of Diazonium Salts," ACS Omega **2**, 1947–1955 (2017).
32. P. Zijlstra, P. M. R. Paulo, K. Yu, Q.-H. Xu, and M. Orrit, "Chemical Interface Damping in Single Gold Nanorods and Its Near Elimination by Tip-Specific Functionalization," Angew. Chem. Int. Ed. **124**, 8477–8480 (2012).
33. D. Ge, S. Marguet, A. Issa, S. Jradi, T. H. Nguyen, M. Nahra, J. Béal, R. Deturche, H. Chen, S. Blaize, J. Plain, C. Fiorini, L. Douillard, O. Soppera, X. Q. Dinh, C. Dang, X. Yang, T. Xu, B. Wei, X. W. Sun, C. Couteau, and R. Bachelot, "Hybrid plasmonic nano-emitters with controlled single quantum emitter positioning on the local excitation field," Nat. Commun. **11**, 3414 (2020).

34. X. Zhou, J. Wenger, F. N. Viscomi, L. Le Cunff, J. Béal, S. Kochtcheev, X. Yang, G. P. Wiederrecht, G. Colas des Francs, A. S. Bisht, S. Jradi, R. Caputo, H. V. Demir, R. D. Schaller, J. Plain, A. Vial, X. W. Sun, and R. Bachelot, "Two-Color Single Hybrid Plasmonic Nanoemitters with Real Time Switchable Dominant Emission Wavelength," Nano Lett. **15**, 7458–7466 (2015).
35. S. Mitiche, S. Marguet, F. Charra, and L. Douillard, "Near-Field Localization of Single Au Cubes: A Group Theory Description," J. Phys. Chem. C. **121**, 4517–4523 (2017).
36. A. Issa, I. Izquierdo, M. Merheb, D. Ge, A. Broussier, N. Ghabri, S. Marguet, C. Couteau, R. Bachelot, and S. Jradi, "One Strategy for Nanoparticle Assembly onto 1D, 2D, and 3D Polymer Micro and Nanostructures," ACS Appl. Mater. Interfaces **13**, 41846–41856 (2021).
37. J. de Torres, P. Ferrand, G. Colas des Francs, and J. Wenger, "Coupling Emitters and Silver Nanowires to Achieve Long-Range Plasmon-Mediated Fluorescence Energy Transfer," ACS Nano **10**, 3968–3976 (2016).
38. C. Deeb, X. Zhou, R. Miller, S. K. Gray, S. Marguet, J. Plain, G. P. Wiederrecht, and R. Bachelot, "Mapping the Electromagnetic Near-Field Enhancements of Gold Nanocubes," J. Phys. Chem. C **116**, 24734–24740 (2012).
39. K. J. Schafer, J. M. Hales, M. Balu, K. D. Belfield, E. W. Van Stryland, and D. J. Hagan, "Two-photon absorption cross-sections of common photoinitiators," J. Photochem. Photobiol. A **162**, 497–502 (2004).
40. C. Deeb, R. Bachelot, J. Plain, A.-L. Baudrion, S. Jradi, A. Bouhelier, O. Soppera, P. K. Jain, L. Huang, C. Ecoffet, L. Balan, and P. Royer, "Quantitative Analysis of Localized Surface Plasmons Based on Molecular Probing," ACS Nano **4**, 4579–4586 (2010).
41. C. Deeb, X. Zhou, J. Plain, G. P. Wiederrecht, R. Bachelot, M. Russell, and P. K. Jain, "Size dependence of the plasmonic near-field measured via single-nanoparticle photoimaging," J. Phys. Chem. C. **117**, 10669–10676 (2013).
42. E. Fišerová and M. Kubala, "Mean fluorescence lifetime and its error," Journal of Luminescence **132**, 2059–2064 (2012).
43. B. Gökbulut and M. N. Inci, "Enhancement of the spontaneous emission rate of Rhodamine 6G molecules coupled into transverse Anderson localized modes in a wedge-type optical waveguide," Opt. Express, OE **27**, 15996–16011 (2019).
44. K. E. Knowles, E. A. McArthur, and E. A. Weiss, "A Multi-Timescale Map of Radiative and Nonradiative Decay Pathways for Excitons in CdSe Quantum Dots," ACS Nano **5**, 2026–2035 (2011).
45. F. M. Gómez-Campos and M. Califano, "Hole Surface Trapping in CdSe Nanocrystals: Dynamics, Rate Fluctuations, and Implications for Blinking," Nano Lett. **12**, 4508–4517 (2012).
46. O. Labeau, P. Tamarat, and B. Lounis, "Temperature Dependence of the Luminescence Lifetime of Single CdSe/ZnS Quantum Dots," Phys. Rev. Lett. **90**, 257404 (2003).
47. P. Spinicelli, S. Buil, X. Quélin, B. Mahler, B. Dubertret, and J.-P. Hermier, "Bright and Grey States in CdSe-CdS Nanocrystals Exhibiting Strongly Reduced Blinking," Phys. Rev. Lett. **102**, 136801 (2009).
48. Y. Peng, S. Jradi, X. Yang, M. Dupont, F. Hamie, X. Q. Dinh, X. W. Sun, T. Xu, and R. Bachelot, "3D Photoluminescent Nanostructures Containing Quantum Dots Fabricated by Two-Photon Polymerization: Influence of Quantum Dots on the Spatial Resolution of Laser Writing," Advanced Materials Technologies **4**, 1800522 (2019).
49. A. Khalid, K. Chung, R. Rajasekharan, D. W. M. Lau, T. J. Karle, B. C. Gibson, and S. Tomljenovic-Hanic, "Lifetime Reduction and Enhanced Emission of Single Photon Color Centers in Nanodiamond via Surrounding Refractive Index Modification," Sci Rep **5**, 11179 (2015).
50. Q. Zhang, G. Li, X. Liu, F. Qian, Y. Li, T. C. Sum, C. M. Lieber, and Q. Xiong, "A room temperature low-threshold ultraviolet plasmonic nanolaser," Nature Communications **5**, 4953 (2014).